3D characterization of the primary Al₃Sc phases in an Al-Sc alloy using Synchrotron X-ray tomography and electron microscopy

Yuliang Zhao ^{a, b*}, Weiwen Zhang ^b, Billy Koe ^{c, d}, Wenjia Du ^c, Mengmeng Wang ^e, Weilin Wang ^e, Elodie Boller ^f, Alexander Rack ^f, Zhenzhong Sun ^a, Jiawei Mi ^c

- ^a Neutron Scattering Technical Engineering Research Centre, School of Mechanical Engineering, Dongguan University of Technology, Dongguan, 523808, P.R. China
- ^b National Engineering Research Centre of Near-net-shape Forming for Metallic Materials, South China University of Technology, Guangzhou, 510641, P.R. China
- ^c Department of Engineering, University of Hull, East Yorkshire, HU6 7RX, UK
- ^d Diamond Light Source, Harwell Science and Innovation Campus, Didcot, Oxfordshire, OX11 0DE, UK
- ^e Shanghai Key Laboratory of Advanced High-Temperature Materials and Precision Forming, School of Materials Science and Engineering, Shanghai Jiao Tong University, Shanghai, 200240, P.R. China
- f ESRF-The European Synchrotron, 71 Avenue des Martyrs, 38000 Grenoble, France Corresponding author: <u>zhaoyl@dgut.edu.cn</u> (Y. Zhao)

Abstract

The three-dimensional structures of the primary Al₃Sc particles in an Al-2%Sc master alloy were studied by synchrotron X-ray microtomography, scanning and transmission electron microscopy. The Al₃Sc phases were found to be a single cube and a cluster of cubes. The surface area, equivalent diameter of the Al₃Sc cubes increased with the increasing of cube volume, but the specific surface area decreases. The primary Al₃Sc cubes and Al-matrix have the same crystal orientation, indicating that the Al₃Sc

phases are the heterogeneous nucleation sites for Al. The experimental results show that α -Al₂O₃ are the possible nucleation sites for the Al₃Sc cubes.

Keywords: Synchrotron X-ray tomography; Aluminium; Scandium; Intermetallic; Microstructure.

Aluminium alloys are widely used in automotive, aerospace and packing industry because of their abundance, high strength-to-weight ratio, good corrosion resistance and excellent recyclability [1]. Grain refinement [2-4] is an effective way to improve both strength and elongation of aluminium alloys. Among all the materials used as Al grain refiners, Sc is one of the most effective elements because it provides the combined effects of (i) grain refinement; (ii) precipitation hardening and (iii) enhanced recrystallization [5-9]. In the Al-Sc master alloys commonly used in industry, L1₂ Al₃Sc primary phases formed and act as heterogenous nucleation sites for α -Al because it has a very small mismatch with α -Al [10]. Sc can be also partially replaced by Zr to form Al₃(ScZr) for the purpose of reducing cost and increasing grain refinement efficiency because Al₃(ScZr) has core-shell type nanostructure which have high-strength and excellent thermal-stability [11-12]. Extensive research has been carried out to study and quantify the addition of Sc in different types of Al alloys, and the enhancement of mechanical properties of Al alloys [13-16].

The size, morphology and distribution of Al₃Sc particles have profound effects on the grain refinement efficiency, castability and mechanical properties of the cast ingots [17-18]. Agglomeration of primary particles in the master alloys leads to the reduction of grain refinement efficiency and has the detrimental effects on the final properties [19]. A full understanding of the particle size, 3D morphology and distribution is essential for developing new strategies to improve the grain refinement and properties

of Al alloys. Current studies of the morphology of the Al₃Sc phases are performed mainly using optical microscope (OM) or scanning electron microscope (SEM), which cannot obtain the true 3D information. For example, Li *et al.* [15] suggested that 3D morphology of Al₃(ScZr) particles are near-globular structures and located within the a-Al matrix or grain boundary. Kastner *et al.* [20] have observed that primary Al₃(ScZr) particles exhibits equi-axes shapes.

Using high-brilliance synchrotron X-ray, it is possible to obtain 3D information for the phases (particles) with the size above ~ 1 micrometre [21]. However, so far, very limited literatures have reported the use of synchrotron radiation X-ray tomography to characterise Al₃Sc phases in Al alloys.

Thus, in this work, we use synchrotron X-ray tomography to study the size, morphology and distribution of the primary Al₃Sc phases in an Al-2%Sc alloy. In addition, scanning and transmission electron microscopy plus electron backscatter diffraction (EBSD) were used complementarily to further quantify the possible nucleation site for the primary Al₃Sc phases and the orientation relationship between primary Al₃Sc phases and Al matrix.

Al-2.0 wt.% Sc master alloy was used in this study. For conventional 2D microstructure characterisation, a Nova SEM 430 Field Emission Gun scanning electron microscope (SEM) equipped with an Oxford energy-dispersive X-ray spectrometer were used. The samples were polished by Ion Beam Milling System Leica EM TIC 3X machine at 5 kV for 2 h and 3 kV for 0.5 h. Some of the sample was deeply etched by the mixture of high-purity iodine and methanol solution (10 g iodine per 100 mL methanol) at room temperature for approximately 4–5 h to dissolve the Al matrix [22]. The sample was cut in a GAIA3 GMU Model 2016 FIB-SEM microscope operated at 5 kV. Crystal orientation and grain size map were obtained using the HKL

Channel 5 EBSD acquisition system. Owing to the similar crystal structure of primary Al₃Sc particle and α-Al matrix, it is impossible to distinguish the two phases using conventional methods. We used the True Phase model embedded in the HKL Channel 5 to distinguish the two phases. For the TEM thin foils, the possible nucleate particles together with the primary Al₃Sc particles were cut and lifted by a tungsten manipulator and transferred to an Omni lift-out cooper grid in a FEI Quanta 3D FEG dual beam microscope. After the transfer, the relatively thick foils on the Cu grid were further thinned by the ion beam step by step to around 80 nm. The foils were then examined in a JEOL 2100F TEM operated at 200 kV.

Synchrotron X-ray tomography experiments were performed at the ID 19 beamline, at the European Synchrotron Radiation Facility (ESRF), in France. The detailed sample parameters used are like the Refs. [23-25]. The imaging system consists of a 25 µm LuAG: Ce scintillator coupled to a white-beam compatible microscope with a 10 × magnification and a high-speed CMOS camera (PCO. DIMAX). The effective pixel size is 1.2 µm and the tomogram scan time is 1 s. For each scan, 1000 projections were acquired over 180° of sample rotation. Tomographic reconstructions were performed on the ESRF cluster using the inhouse developed software-package PyHST_2. Fig. s1a shows the typical image processing procedures and methods employed for 3D microstructure determination. As showed in Fig. s1b, the grey block phases were identified as Al₃Sc. Both X-ray and SEM images show that the primary Al₃Sc particles exhibit square and triangular shapes in 2D. Open source image processing software, Image J [26] was used to adjust the contrast between the different phases. Then, the 3D bilateral filter was applied to the tomography datasets to increase the contrast and reduce noise. Finally, the primary Al₃Sc particles and Al dendrites, were manually trimmed for the different material phases. 3D segmentation and feature rendering were performed using Avizo Lite v9.0.1 (VSG, France). Typically, a sub-volume of 200^3 voxels with a voxel size of $(1.2 \,\mu\text{m})^3$ was chosen for further analyses.

The two parameters were used to characterize the surface curvature, the mean curvature H, Gaussian curvature K [27] is defined as:

$$H = 0.5 * \left(\frac{1}{R_1} + \frac{1}{R_2}\right) \tag{1}$$

$$K = \left(\frac{1}{R_1 * R_2}\right) \tag{2}$$

where R_1 and R_2 are the two principal radii of curves respectively. Local curvature is an important geometrical parameter for the interface between two phases (dendrites or intermetallic) formed during the solidification processes, influencing the diffusion of solutes and therefore the final morphology of the phases. We used the skeletonization function available in Avizo® [28] to peel off the 3D structures of the primary Al₃Sc particles down to a skeleton (1-voxel thickness) with connecting nodes. The length of the curve between each node, and the number of the connecting nodes can be calculated, and therefore the 3D characteristics of skeleton. The equivalent diameters D_{eq} is defined as average equivalent diameters of the different particles of the considered phase and the volume V represents the whole volume of considered phase [29]

$$D_{eq} = \sqrt[3]{\frac{6V}{\pi}} \tag{3}$$

The other important parameter specific surface area (SSA) is defined as surface area A per unit volume V [30]:

$$SSA = \frac{A}{V} \tag{4}$$

Fig. 1 shows the 3D rendering of primary cubic Al_3Sc particles in the volume (240 $\mu m \times 240 \ \mu m \times 240 \ \mu m$). It can be seen that, from Fig. 1a, most of these particles were found to form clusters with several cubic faceted morphologies. Conglomeration of the clusters in the matrix is also observed in the Ref. [10-11, 18]. The primary Al_3Sc

particles are firstly formed in the Al-2Sc alloy during solidification, owing to the Sc content is greater than the eutectic composition (0.55% Sc) [8]. Figs. 1b-c show the mean curvature and gaussian curvature of primary Al₃Sc particles, the red colour of cubic edge of particles illustrating the cusped-cubic morphologies of these particles. Fig. 1d shows the distribution of mean curvature and gaussian curvature of primary Al₃Sc particles, indicating both follow gaussian distribution. The distribution peak position (μ) of mean curvature and gaussian curvature of primary Al₃Sc particles are 0.06 and 0.14, respectively, and the standard deviation (σ) of these particles are 00.06 and 0.14, respectively. This indicates that the cubic primary Al₃Sc particles has the cusped edge. Fig. 1e and f show the skeletons of primary Al₃Sc particles and their node length distribution, respectively. The node length of these particles also follows the gaussian distribution and their length are in the range of 5-20 μ m. *Much richer and cleaner information, mean and gaussian curvature and skeletons of primary Al₃Sc phases in different view angles are demonstrated in the accompanying video.*

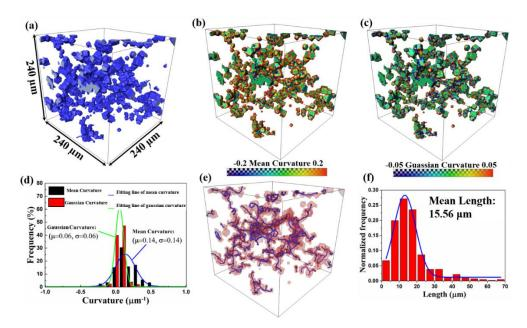


Fig. 1 3D characterization of primary Al₃Sc phases in a volume of 240 μm × 240 μm
× 240 μm: (a) 3D reconstructed particles; (b) mean curvature; (c) gaussian curvature;
(d) distribution of mean curvature and gaussian curvature; (e) particles using the skeletonization function; (f) statistical analysis of node length.

Typical Al₃Sc morphologies found in the Al-2Sc alloy and their statistical analysis are shown in Fig. 2. The cubic primary Al₃Sc particles are in contact with each other, which can be clearly seen in both 3D rendered structures and deep-etched SEM images (Fig. 2a). New particles generally nucleate preferentially at the corners or edges of preexisted particles during the growth of primary Al₃Sc particles. This arises because at the particle corners there will be a locally thinner Sc depleted layer ahead of the interface, resulting in higher gradients of constitutional undercooling [31]. Fig. 2b shows the 3D rendered structures and deep-etched SEM images of single Al₃Sc particles. From the deep-etched SEM images, the Al₃Sc is a typical cubic structure with three perpendicular ledges at the corner. The side length of this single cubic Al₃Sc particles is about 25 µm. In some case, there are some holes in the centre-facet of the cubic (Fig. 2c). This similar was also observation in the [17]. This is attributed to the growth of primary Al₃Sc particles interface had become locally unstable. Li et al. [32] suggested that the central hole of the particle may generate during mechanical grinding and polishing. From the 3D tomography images (Fig. 2c), the central hole is formed during solidification because of the non-destructive nature of synchrotron X-ray tomography. The statistical analysis of Al₃Sc cluster and single Al₃Sc particle is shown in the Figs. 2d-g. The Fig. 2d shows the volume of Al₃Sc cluster is mainly in the range of 5000-80000 µm³ and the insert image shows the volume of single Al₃Sc particles is mainly in the range of 1000-4000 μm³. This further confirms that the Al₃Sc cluster have a large volume. The next graph (Fig. 2e) shows that volume of primary Al₃Sc particles increased with increasing surface area. They follow the linear relationship: Y = -1098+ 2.5*X and single Al₃Sc particles are mainly located in the left corner of the figure. This indicating that the Al₃Sc with increased surface area is a good grain refiner. In the Fig. 2f, the equivalent diameter of primary Al₃Sc particles (including Al₃Sc cluster and

single Al_3Sc particle) is plotted against the volume for the Al-2Sc master alloy. The equivalent diameter of primary Al_3Sc particles increased with volume and follow nonlinear relationship: $Y = 1.24*X^{3.33}$. Fig. 2g shows the volume primary Al_3Sc particles plotted against the specific surface area. Their distribution is almost random. While the larger the volume of primary Al_3Sc cluster, the smaller its specific surface area. This means that the increase of volume resulting in the reducing of surface area of Al_3Sc cluster and become relatively compacted.

Fig. 3a exhibits the EBSD images of the alloy containing primary Al₃Sc particles. Owing to the similar crystal structure of Al and Al₃Sc (their mismatch in lattice parameter is 1.34% [8]), it is impossible to distinguish two phases using normal EBSD analysis. The True Phase model embedded in the HKL Channel 5 using to identify the two phases, as shown in Fig. 3b, which is combined with SEM-EDS analysis crystal structure of Al₃Sc phase and Al matrix in the alloy. The Kikuchi patterns of Al₃Sc and Al phases are shown in the Figs. 3c-d. The calculation of Euler angles (φ_1 = 210.0, φ_2 = 43.2, φ_3 = 82.8) displayed in Fig. 3c for Al₃Sc phase, and Euler angles (φ_1 = 80.1, φ_2 = 16.0, φ_3 = 86.0) displayed in Fig. 3d for Al matrix. Mean angular deviation (MAD) is the difference value between the experimental and calculated patterns of the particles calculated by the EBSD software. Usually, the value for MAD is lower than 0.7, which means that the identified particle can be accepted by the calculated patterns of the particle [33]. The Al₃Sc phase is formed at 659 °C during a eutectic reaction, has a cubic ordered structure of L12 type with a = 0.4104 nm. The EBSD results of Al-2Sc alloy is shown in Fig. 3e. This figure shows that the primary Al₃Sc particles and Al matrix have the same crystal orientation, which indicating that the Al₃Sc particles provide the heterogeneously nucleation site for Al matrix. This result is accordance with previous studies [10, 17-18]. The graph inserted in Fig. 3e displays that the grain

size distribution of the alloy is mainly in the range of 20-80 μm and the average grain size is 41.60 μm .

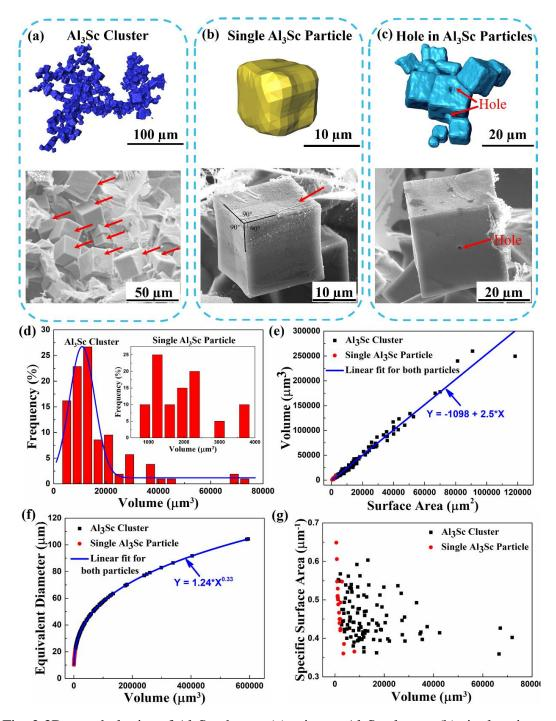


Fig. 2 3D morphologies of Al₃Sc phases: (a) primary Al₃Sc cluster; (b) single primary Al₃Sc particles; (c) holes in Al₃Sc particles; (d) volume distribution of Al₃Sc cluster (insert graph: single Al₃Sc phases); (e) the surface area of Al₃Sc particles as a function of volume; (f) the volume of Al₃Sc particles as a function of equivalent diameter; (g) the relationship between the volume of Al₃Sc particles and specific surface area.

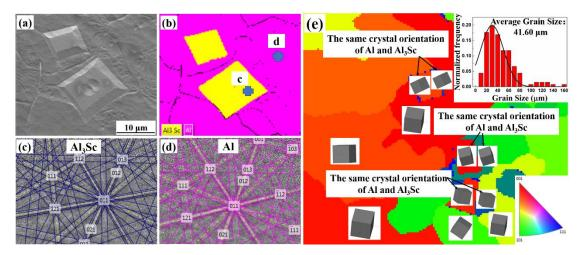


Fig. 3 EBSD analysis of Al₃Sc phases: (a) band contrast image; (b) EBSD image showing the phases using True Phase model; (c-d) Kikuchi patterns of Al₃Sc and Al phases; (e) EBSD images presents that the Al₃Sc in Al grains showing the same crystal orientation, insert graph shows the grain size distribution of Al matrix in the alloys.

In order to determine the possible nucleation site for Al₃Sc particles, FIB-TEM were performed on the sample. The detailed procedure for cutting the TEM sample can be found on the Fig. s2. Fig. 4(a) shows the region containing aluminium oxides, Al₃Sc particles and Al matrix, which were cut by ion beam. In order to further confirm their phase structure, the Al₃Sc particles/Al matrix interface (region A) and aluminium oxides/Al₃Sc particles interface (region B) were studied by TEM. The crystal structure of Al₃Sc particles and Al phase were identified by selected area diffraction pattern (SADP), as shown in Fig. 4(b). There are many tiny circle-Al₃Sc particles existed in the Al-side of Al₃Sc particles/Al matrix interface, which was confirmed by the TEM-EDS (Fig. 4(c-d)). The aluminium oxides/Al₃Sc particles interface was shown in the Fig. 4(e). As the TEM-EDS line mapping (Fig. 4(f-h)) indicating that the TEM results show that Al₂O₃ provides the nucleation site for Al₃Sc particles. The graph inserted in the Fig. 4f indentation the structure of the aluminium oxides is the α-Al₂O₃. The SEM-EDS line mapping (Fig. 4(i-j)) further confirms this result. A high density of stacking

faults was observed on the Al₃Sc particles-side of aluminium oxides/Al₃Sc particles (Fig. 4k).

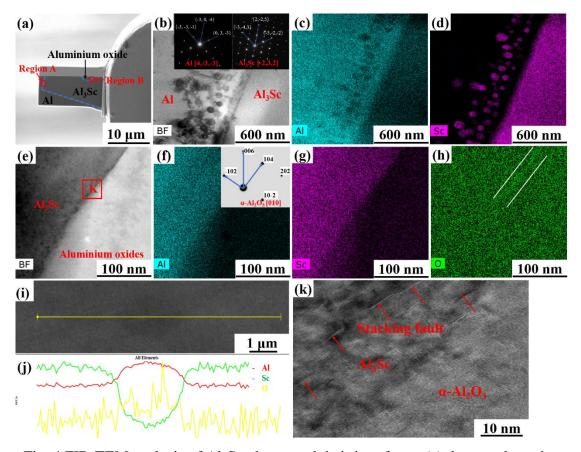


Fig. 4 FIB-TEM analysis of Al₃Sc phases and their interfaces: (a) the sample region contains aluminium oxides, Al₃Sc particles and Al matrix, which has been cut by ion beam; (b) Al₃Sc particles/Al matrix interface; (c-d) EDS mapping of (b); (e) aluminium oxides/Al₃Sc particles interface; (f-h) EDS mapping of (e); (i-j) EDS line mapping of aluminium oxides/Al₃Sc particles interface; (k) stacking faults on the Al₃Sc particles-side of α-Al₂O₃/Al₃Sc particles interfaces.

In this paper, the 3D structures of primary Al_3Sc phases in an Al-2%Sc master alloy were studied by synchrotron X-ray microtomography and electron microscopy. It was found that high mean and gaussian curvature of primary Al_3Sc phases are mainly at the edges and corners of the cubes. The skeletonization analysis shows that the node length between two cubes was in the range of 5-20 μ m. The primary Al_3Sc phases are either form a cluster (volume: 5000-80000 μ m³), or in a single cube (volume: 1000-4000

 μm^3). The surface area, equivalent diameter of Al₃Sc cubes increases with increasing volume, but the specific surface area decreases. The TEM investigation confirms that α -Al₂O₃ are the potential nucleation site for Al₃Sc phases.

Acknowledgements

This work was supported by UK-EPSRC grants (EP/L019965/1); the Team project of Natural Science Foundation of Guangdong Province (2015A030312003); Open Funds of National Engineering Research Centre of Near-Net-Shape Forming for Metallic Materials (2018014); Science and Technology Project of Zhaoqing (2018K009); and Scientific Research Foundation of Advanced Talents (Innovation Team), DGUT (No. KCYCXPT2016004). We also would like to acknowledge the European Synchrotron Radiation Facility, ESRF, France, for provision of synchrotron radiation beamtime on the ID19 beamline under proposal number MA 3752.

Reference

- [1] J.G. Kaufman, E.L. Rooy, Aluminum Alloy Castings: Properties, Processes, and Applications, ASM International, Materials Park, OH, 2004.
- [2] M.A. Easton, M. Qian, A. Prasad, D.H. StJohn, Curr. Opin. St. M. 20 (2016) 13-24.
- [3] R.G. Guan, D. Tie, Acta Metall. Sin. (Engl. Lett.) 30 (2017) 409-432.
- [4] Z.L. Liu, Metall. Mater. Trans. A 48A (2017) 4755-4776.
- [5] S. Riva, K.V. Yusenko, N.P. Lavery, D.J. Jarvis, S.G. Brown, Inter. Mater. Rev. 61 (2016) 1-26.
- [6] D.G. Eskin, Sc Applications in Aluminum Alloys: Overview of Russian Research in the 20th Century, in O. Martin (Ed.), Light Metals 2018, Springer, Cham. 2018, p. 1565.
- [7] J. Røyset, N. Ryum, Inter. Mater. Rev. 50 (2005) 19-44.

- [8] T. Dorin, M. Ramajayam, A. Vahid, T. Langan, Aluminium Scandium Alloys, in Roger Lumley (Ed.), Fundamentals of Aluminium Metallurgy, Woodhead Publishing, 2018, p 439.
- [9] J. Röyset, Metall. Res. Technol., 25 (2013) 11-21.
- [10] A.F. Norman, P.B. Prangnell, R.S. Mcewen, Acta Mater. 46 (1998) 5715-5732.
- [11] P.W. Voorhees, Nat. Mater. 5 (2006) 435-436.
- [12] E. Clouet, L. Laé, T. Épicier, W. Lefebvre, M. Nastar, A. Deschamps, Nat. Mater., 5 (2006) 482-488.
- [13] S.A. Zhou, Z. Zhang, M. Li, D.J. Pan, H.L. Su, X.D. Du, P. Li, Y.C. Wu, Mater. Des. 90 (2016) 1077-1084.
- [14] W. Prukkanon, N. Srisukhumbowornchai, C. Limmaneevichitr, J Alloys Comp. 477 (2009) 454-460.
- [15] J.H. Li, B. Oberdorfer, S. Wurster, P. Schumacher, J. Mater. Sci. 49 (2014) 5961-5977.
- [16] G.B. Teng, C.Y. Liu, Z.Y. Ma, W.B. Zhou, L.L. Wei, Y. Chen, J. Li, Y.F. Mo, Mater. Sci. Eng. A 713 (2018) 61-66.
- [17] K.B. Hyde, A.F. Norman, P.B. Prangnell, Acta Mater. 49 (2001) 1327-1337.
- [18] C. Xu, R. Du, X.J. Wang, S. Hanada, H. Yamagata, W.H. Wang, T. Nonferr. Metals Soc. 24 (2014) 2420-2426.
- [19] F. Chen, F. Mao, Z.N. Chen, J.Y. Han, G.Y. Yan, T.M. Wang, Z.Q. Cao, J. Alloys Comp. 622 (2015) 831-836.
- [20] J. Kastner, B. Harrer, H.P. Degischer, Mater. Charact. 62 (2011) 99-107.
- [21] P. Pietsch, V. Wood, Annu. Rev. Mater. Res., 47 (2017) 451-479.
- [22] W. Zhang, B. Lin, Z. Luo, Y. Zhao, Y. Li, J. Mater. Res. 30 (2015) 2474-2484.
- [23] Y. Zhao, W. Du, B. Koe, T. Connolley, S. Irvine, P.K. Allan, C.M. Schlepütz, W. Zhang, F. Wang, D.G. Eskin, J.Mi, Scr. Mater. 146 (2018) 321-326.
- [24] Y.L. Zhao, Z. Wang, C. Zhang, W.W. Zhang, J. Alloy. Compd. 777 (2019) 1054-1065.
- [25] Y.L. Zhao, D.F. Song, B. Lin, C. Zhang, D.H. Zheng, S. Inguva, T. Li, Z.Z Sun, Z. Wang, W.W. Zhang, Mater. Charact. 153 (2019) 354–365.
- [26] C.A. Schneider, W.S. Rasband, K.W. Eliceiri, Nat. Methods 9 (2012) 671–675.
- [27] R. Mendoza, J. Alkemper, P. W. Voorhees, Metall. Mater. Trans. A 34 (2003) 481-489.

- [28] Thermo Scientific Avizo Software 9 User's Guide, Thermo Fisher Scientific, 2018. https://www.fei.com/WorkArea/DownloadAsset.aspx?id=34359741225
- [29] J. Wang, Z.P. Guo, S. M. Xiong, Mater. Character. 123 (2017) 354-359.
- [30] D. Kammer, P.W. Voorhees, Acta Mater. 54 (2006) 1549-1558.
- [31] M.C. Fleming, Solidification Processing. McGraw-Hill, London, 1974.
- [32] Y.K. Li, X.D. Du, J.W. Fu, Y. Zhang, Z. Zhang, S.A. Zhou, Y.C. Wu, Arch. Foundry Eng., 18 (2018) 51-56.
- [33] M.V. Kral, H.R. McIntyre, M.J. Smillie, Scr. Mater. 51 (2004) 215-219.